Machine learning for beam correction study of the injection beamline at Wuhan Advanced Light Source*

Hui Wang,[1,2] Hao-Hu Li,[3] Jia-Bao Guan,[1,2] Yuan Chen,[1,2] Ji-Ke Wang,[1,2] Yuan-Cun Nie,[1,2,†] and Jian-Hua He[1,2]

[1]*The Institute for Advanced Studies, Wuhan University, Wuhan 430072, China*
[2]*Advanced Light Source Research Center, Wuhan University, Wuhan 430072, China*
[3]*Shanghai APACTRON Particle Equipment Co.Ltd, Shanghai 201800, China*

As a fourth-generation synchrotron radiation light source working at 1.5 GeV, Wuhan Advanced Light Source (WALS) is being designed, which uses a full-energy linear accelerator (LINAC) as its electron beam injector. The injection beamline adopts a three-stage scheme: firstly, the beam from the LINAC that is 6 m under the storage ring is horizontally deflected below the storage ring, then it gradually climbs from underground to the same altitude as the storage ring, and finally the beam is delivered horizontally into the injection straight section inside the storage ring. Meanwhile, the Twiss parameter matching between the LINAC and storage ring is completed. During the construction of the beamline, magnet manufacturing errors, installation errors and beam injection errors from the LINAC will cause beam deviations from predetermined ideal orbits, and even particle losses. As a result, the electron beam correction is required during beam commissioning. Different from the single-direction beam correction of general transfer lines, the horizontal and vertical directions of the beam are coupled in the WALS injection transfer line, which greatly increases the complexity and difficulty of beam correction. Machine learning technology has been developed extensively in recent years, and its powerful algorithm of invertible neural network model is expected to be able to solve the beam commissioning difficulty of the beam injection transfer line at the WALS. Therefore, an invertible neural network model has been designed and trained to simulate the beam transport and beam correction of the WALS injection beamline. By optimizing the number and location of beam profile diagnostics, the accuracy of bidirectional prediction and beam correction effect can be greatly improved. The method is of great practical significance for the commissioning and operation of similar complex beam transport systems.

Keywords: Beam correction, Injection transfer beamline; Machine learning; Beam dynamics; Invertible neural network

I. INTRODUCTION

Synchrotron radiation light sources are large-scale facilities for observing and studying the microscopic world using the phenomenon of synchrotron radiation [1], and accelerators are important parts of the Synchrotron radiation light sources. After decades of development, they have evolved from the first generation as part-time light sources that simply use synchrotron light generated from particle accelerators, to the fourth generation of diffraction-limited storage ring light sources that have ultra-low beam emittance and adopt a large number of undulator insertions. A number of fourth-generation synchrotron radiation light source facilities are in operation or under construction around the world. The MAX IV in operation in Sweden uses multi-bent achromat (MBA) lattices to reduce the beam emittance to below 0.1 nm·rad and increase the brightness by 2 orders of magnitude [2]. Brazil's Sirius achieves lower beam natural emittance compared to MAX IV through stronger horizontal focusing [3]. ESRF-EBS in Europe is the world's first 6 GeV storage ring light source upgraded from ESRF, which significantly enhances its brightness and coherence [4]. HEPS [5], HALF [6] and several other fourth-generation synchrotron radiation light sources are under construction. Synchrotron radiation light sources have been widely applied in the fields of physics, materials chemistry, biology, life sciences, electronic information engineering and so on [7].

Wuhan Advanced Light Source (WALS), which is currently under design, is a fourth-generation diffraction-limited synchrotron radiation light source with a 1.5 GeV full-energy linear accelerator (LINAC) as its injector [8]. The electron beams are transported to the 1.5 GeV storage ring via beam injection transfer line (BITL) [9–11]. To accommodate the future construction of a 4.0 GeV storage ring, the LINAC is 6 m underground and laterally offset relative to the 1.5 GeV storage ring. Since the LINAC is 6 m under the storage ring, the WALS BITL adopts a "three-stage" design scheme: at first, the beam is horizontally deflected below the storage ring, then it gradually climbs from the underground tunnel to the same altitude level as the storage ring, completing a vertical climb with a height of 6 m, and finally the beam is transferred horizontally into the injection straight section inside the storage ring [12]. The special design scheme makes the horizontal and vertical beam coupling occur when the beam is transported. Especially for the dispersion function, the two transverse directions need to be considered and corrected simultaneously when the beam is commissioned. For such complex beam dynamics problem, where beam diagnostics equipment is limited in practical, neither the traditional beam commissioning method, like the SVD (Singular Value Decomposition) linear fitting algorithm [13–16] nor a global beam commissioning method [12] proposed for the WALS BITL, is optimal to adopt. It is thus necessary to take the advantages of the machine learning algorithm to simulate the beam transport and perform horizontal and vertical beam corrections simultaneously for the WALS BITL.

* Supported by the by the Major Science and Technology Project of Hubei Province (2021AFB001)

† Corresponding author, nieyuancun@whu.edu.cn

In recent years, machine learning algorithm has been widely applied in the field of accelerator physics. The multi-hidden layer structure of neural networks and the algorithmic activity provided by the activation functions can accurately realize the beam dynamic simulations of particle beams in accelerators. Applications of machine learning have been reported at many light sources. For example, SLAC National Accelerator Laboratory trained two independent neural network constructs at its Linac Coherent Light Source (LCLS) [17, 18], to achieve accurate prediction of 2D images of electron bunches [19]. Shanghai Synchrotron Radiation Facility (SSRF) [20–23] used machine learning to extract beam information bunch by bunch and correct beam orbits of the storage ring [24]. Using convolutional neural network (CNN) [25, 26], the National Synchrotron Radiation Laboratory (NSRL) at the University of Science and Technology of China (USTC) successfully fitted and calculated the beam cross-section dimensions by noise suppression of the collected beam images [27]. In addition, online correction using Lasso regression [28, 29], and Beta function correction using neural network have been carried out [30]. More and more light sources are using machine learning algorithms to solve problems in the field of accelerator physics [31, 32].

In our study, an invertible neural network (INN) [33, 34] containing 8 affine coupling modules [35] has been successfully designed after many tests, where the ReLU (Rectified Linear Unit) activation function [36, 37] is applied, and the Adam (adaptive moment estimation) algorithm [38] and the Back-propagation algorithm [39, 40] are introduced. By learning the dataset consisting of two group of variables, where one group is the magnet K-value of (m^{-2}) quadrupole magnets with adjustable electric current in the WALS BITL (as input x), and another group is the horizontal (σ_x) and vertical (σ_y) beam size collected at beam profile monitoring systems (as output y), not only the forward prediction from the magnet K-value to the beam size σ, but also the inverse prediction from the beam size σ to the magnet K-value can be realized. The AT toolbox in MATLAB has been used to model the WALS BITL, collect the beam related data, verify the inverse prediction results of the INN model. Optimization of the beam correction has been successfully realized in simulation for the WALS BITL.

The following content of this paper is divided into five sections. Sec. II introduces the layout of the WALS BITL, as well as the global beam correction method proposed at the beginning of the beamline design. Sec. III introduces the INN model designed for the WALS BITL, which is described from six aspects: model structure assumption, beam correction process, placement and quantity setting of beam profile monitoring systems, datasets making, model structure setup and training results. Sec. IV is to verify the beam correction method of the INN model. Sec. V is the analysis of the beam correction method, where the dynamic relationship of the method, the definition of the loss function and the selection of evaluation indicators are introduced. Summaries and conclusions of the work are described in the Sec. VI.

II. THE WALS BITL AND GLOBAL BEAM CORRECTION

A. Design of the WALS BITL

For synchrotron radiation light sources, the injection transfer line is required to deliver the electron beam into the storage ring with high quality and high transmission efficiency. Stable operation of a synchrotron radiation light source highly relies on precise design and construction of the injection transfer line. When design the transfer line, one needs to ensure that the Twiss parameters of the beam are accurately matched, and the dispersion functions are under control. At the same time, considering the installation errors, injection errors from the LINAC, magnet manufacturing errors and many other factors during the beamline construction, it is necessary to perform beam correction on the basis of theoretical design. In general, beam diagnostic devices such as BPMs [41] and beam profile monitoring systems are placed along the beamline to collect beam information, and horizontal/vertical correction (HVC) magnets are arranged for beam orbit corrections.

At the WALS, the BITL consists of three sections as mentioned earlier. The first section of the transfer line is designed with two 15° dipole magnets and three quadrupole magnets to form a horizontal achromatic unit, supplemented by ten quadrupole magnets for beam envelope manipulation. In the second section, the beam is deflected 30° vertically, climbing over the 6 m slope, and then deflected back by 30° to arrive the same horizontal plane as the storage ring. Both ends of the second section are designed with two 15° dipole magnets and three quadrupole magnets to form a vertical achromatic unit. The two vertical achromatic units in the second section adopt the same magnet parameters as in the horizontal achromatic unit in the first section, to reduce the complexity of beam commissioning. In the third section, four quadrupole magnets are used to deliver the beam from the transfer line to the entrance of the storage ring. A horizontal achromatic unit consisting of two 10.5° dipole magnets, injection septum, and three quadrupole magnets is used to match the Twiss parameters. Fig. 1 plots the 3D model of the WALS BITL. Fig. 2 shows the evolution of Twiss parameter along the WALS BITL, with the Beta function not exceeding 25 m and the dispersion function not exceeding 0.6 m. Fig. 3 presents the beam size in the BITL. Beam size refers to the standard deviation of the electron beam bunch that follows a Gaussian distribution.

B. Global Correction Method

During beamline construction, there are installation errors, manufacturing errors and many other errors that will cause the particle beam not to follow the predetermined orbit, leading to Twiss parameter mismatch and even beam losses. So it is necessary to optimize the beam correction of the beamline. The global correction method is a beam correction method applied in the design of the WALS BITL [12]. Considering the horizontal-vertical coupling problem of the WALS BITL,

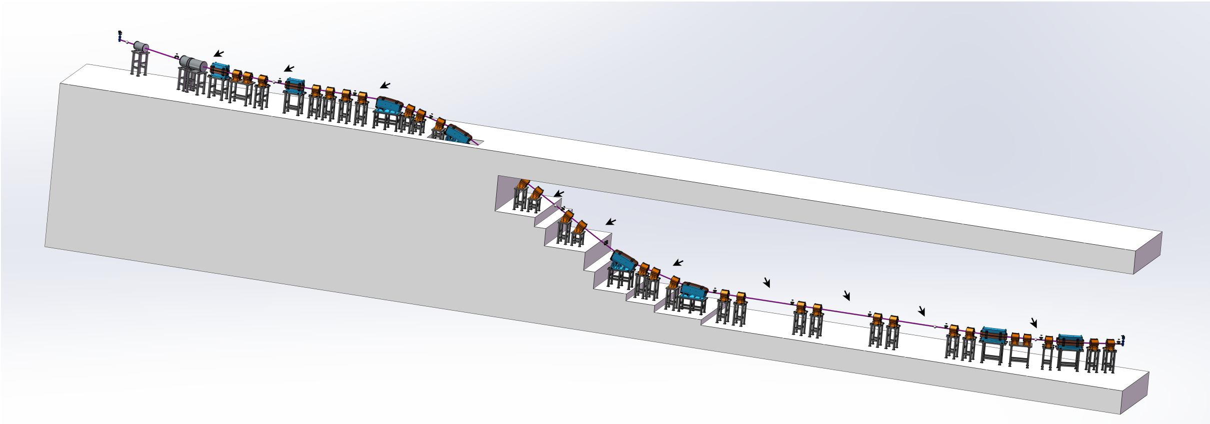

Fig. 1. 3D model image of the WALS BITL. Arrows indicate the potential location for the placement of the beam profile monitoring systems.

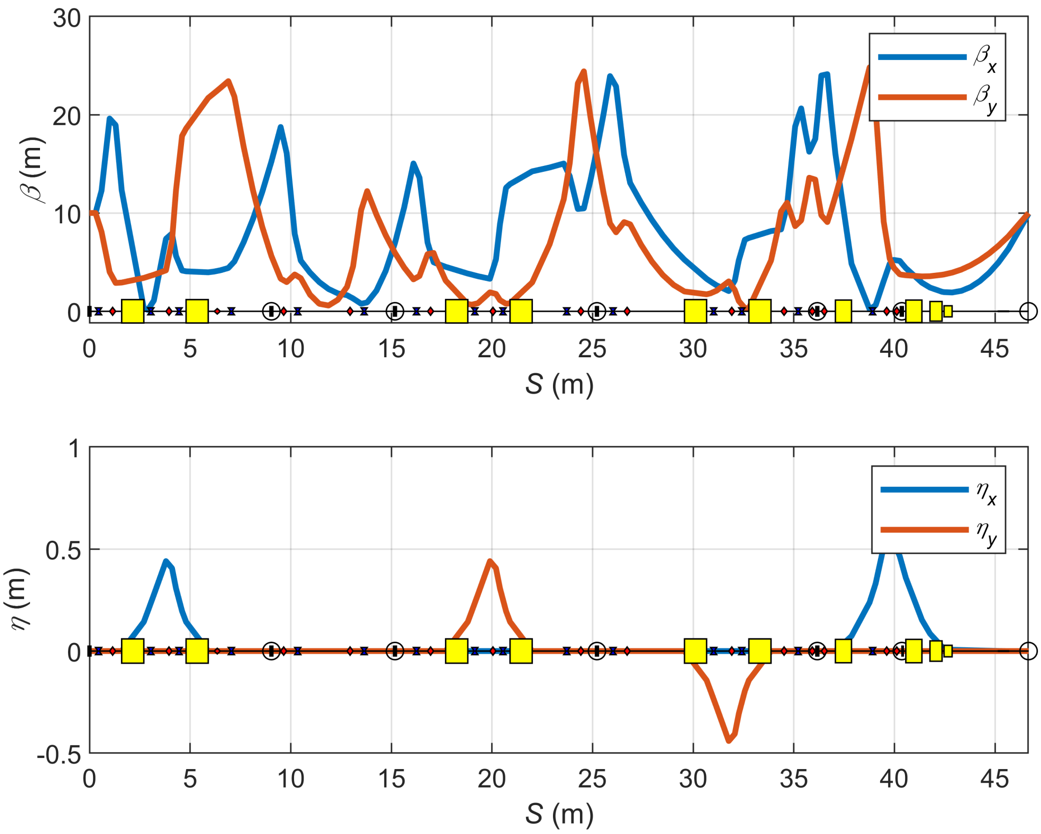

Fig. 2. Twiss parameters (β and η) along the WALS BITL. In the beamline, the dark blue boxes represent the HVC correction magnets, the yellow boxes represent the dipole magnets, the circles represent the BPMs, and the rest represents the quadrupole magnets.

especially for the correction of the dispersion function, it is essential to correct both the horizontal and vertical directions at the same time, so the global correction method is proposed at first for the beam correction.

The process of global correction method includes two parts: orbit correction and optical correction. Orbit correction is achieved with six sets of HVC magnets and BPMs placed in pairs. In Fig. 2 or Fig. 3, the specific locations of the HVCs and BPMs can be observed. Optical correction is realized by using the AT toolbox simulation on MATLAB, which includes randomly generating 20-50 sets of quadrupole magnets seeds to test the parameters, retaining the seeds with better results (such as lower maximum beta function, lower dispersion function at the end of the beamline), and iterating again until the ideal quadrupole setting is found. By employing this overall computational approach, simultaneous bidirectional beam correction can be realized in simulation. Since the quadrupole magnets of the WALS BITL are powered in-

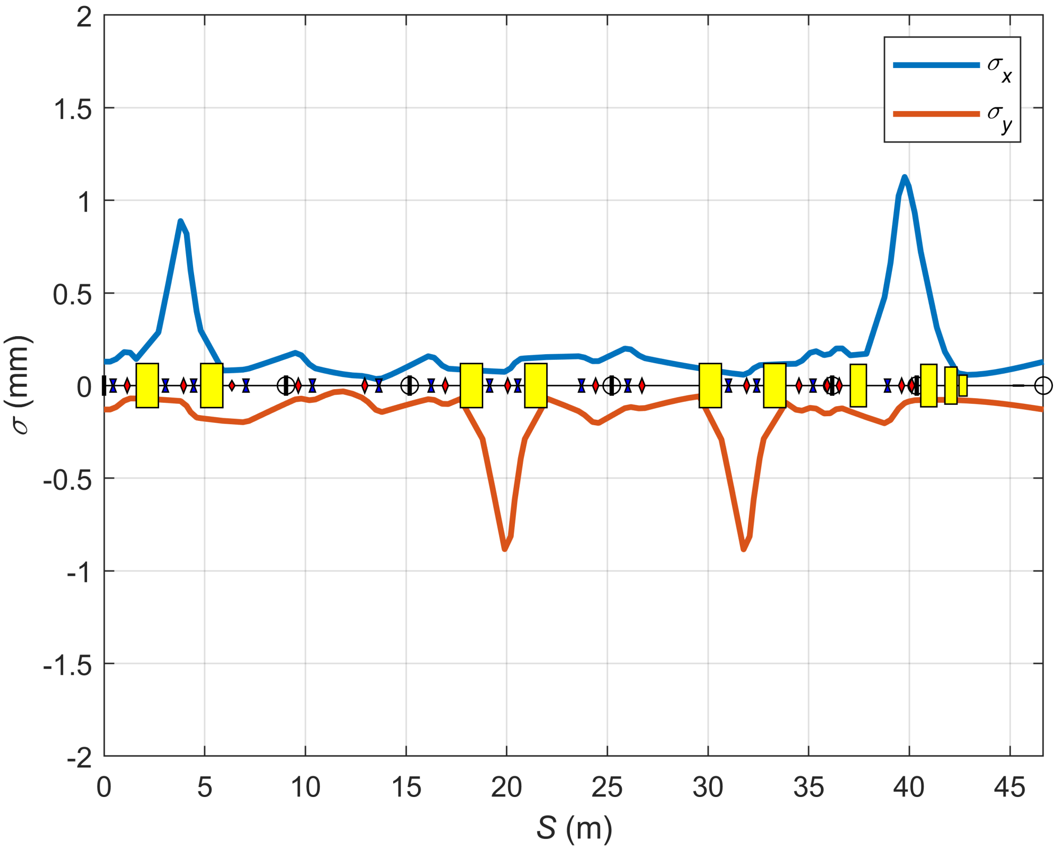

Fig. 3. Beam size along the WALS BITL. In the beamline, the dark blue boxes represent the HVC correction magnets, the yellow boxes represent the dipole magnets, the circles represent the BPMs, and the rest represents the quadrupole magnets.

dividually, the 18 quadrupole magnets in the non-dispersion region and the 12 quadrupole magnets in the dispersion region (30 in total) can be adjusted separately. Twenty error seeds were randomly generated, and the beam optics parameters and beam sizes under different error seeds were analyzed. In the global correction simulations, the orbit correction has been carried out with the help of 6 sets of HVC magnets and BPMs, while the optical correction has been realized by using MATLAB calculations, where beam information along the beamline was collected and applied for the optical correction.

Fig. 4 shows the comparison before and after beam orbit correction, where x represents the horizontal orbit and y represents the vertical orbit. The curves correspond to 20 error seeds mentioned earlier. Comparing (a) and (b), it is observed that the maximum error in the horizontal direction of the orbit before correction is 22 mm, with the end values ranging from -18 mm to 12 mm. After correction, the maximum error in the orbit is reduced to 2.7 mm, and the end values are nearly 0 mm (ideal orbit). Similarly, by comparing (c) and (d), it is found that the maximum error in the vertical direction of the orbit before correction is 27 mm, with the end values ranging from -11 mm to 16 mm. After correction, the maximum error in the orbit becomes 2.7 mm, and the end values are also close to 0 mm. It can be seen that the positions and directions of the orbit at the injection point have been basically corrected ideally.

For the beam optics parameters, Fig. 5 plots the results before correction, and Fig. 6 presents the results after correction. The curves also correspond to 20 error seeds mentioned earlier. By comparing Fig. 5 and Fig. 6, it is found that after correction, the maximum value of β_x at the end decreases from 17.8 m to 12.6 m. For β_y, the maximum value at the end decreases from 12.3 m to 10.4 m. The maximum value of η_x at the end decreases from 0.5 m to 0.01 m, and the maximum value of η_y at the end decreases from 0.4 m to 0 m. Overall, the beta function at the end is close to 12 m, and the dispersion function is close to 0 m, meeting the correction requirements of 15 m and 0.2 m, respectively.

To compare with the INN method, 20 new seeds were selected for correction using the global method. These 20 seeds are different from the previous 100 seeds [12] and have a slightly smaller error range. The global correction achieved similar results to the previous study. The correction of dispersion function, especially its deviation in the middle part of the beamline, was a key focus in the previous work, resulting in better overall correction. However, the correction results at the injection point of the injection straight section inside the storage ring were very close to each other.

The global correction method achieves beam correction for

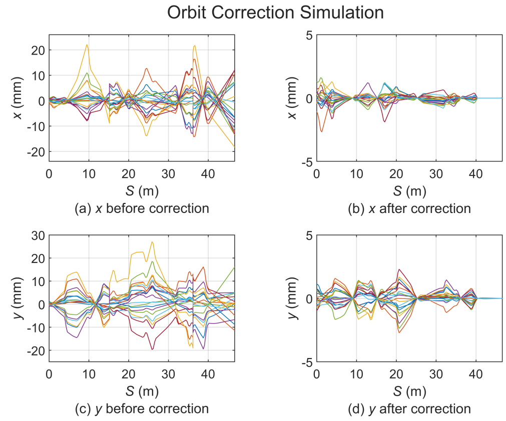

Fig. 4. Global correction method: comparison before and after beam orbit correction. (a) and (b) represent x-orbit before and after correction, (c) and (d) represent y-orbit before and after correction.

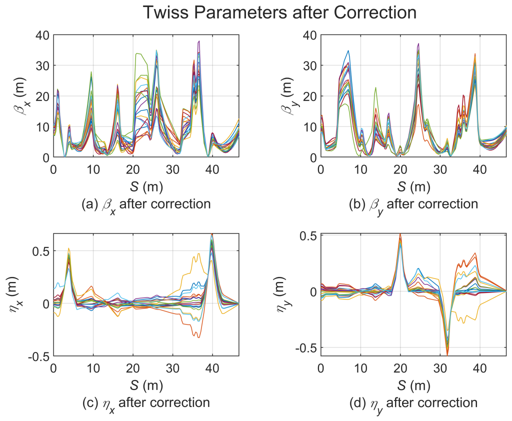

Fig. 6. Global correction method: beam optics function after correction. (a)represents β_x after optical correction, (b)represents β_y after optical correction, (c)represents η_x after optical correction, and (d)represents η_y after optical correction.

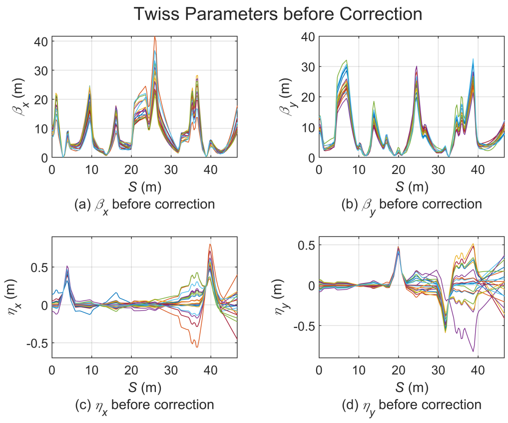

Fig. 5. Global correction method: beam optics function before correction. (a)represents β_x before optical correction, (b)represents β_y before optical correction, (c)represents η_x before optical correction, and (d)represents η_y before optical correction.

the WALS BITL because it captures information from all points along the transport line in simulations. However, in reality, there are limited locations where the beam diagnostic elements can be placed, and the available information during the actual beam correction is far less than that in simulations. As a conclusion, the global correction method is not available in actual beam correction. So it is necessary to develop a new beam commissioning method, which can not only solve the problem of horizontal and vertical beam corrections at the same time, but also can complete the beam correction under limited information. Therefore, we have attempted to study the beam correction of the WALS BITL by using machine learning algorithms.We propose and implement the use of an INN model for beam correction of the WALS BITL.

III. INVERTIBLE NEURAL NETWORK MODEL

With the continuous progress of artificial intelligence, machine learning systems have been developing rapidly [42]. More and more people are trying to use machine learning technology for cutting edge researches [43–46], especially in physics [47–50]. In the field of particle accelerators, applications of machine learning technology in beam commissioning are under rapid development as well.

A. Network Structure for the WALS BITL

At present, machine learning algorithms are often used to design storage rings or study beam instabilities, where the number of hidden layers of neural networks designed are generally ranging from one to three, while the number of nodes ranges from tens to thousands. Multi-objective genetic algorithm [51, 52] are usually applied to find the best working point of each component of particle accelerators. In our case, beam transport at the WALS BITL is unidirectional, there are few adjustable components, and the three-stage beamline design is very specific. As a result, it is necessary to design a unique neural network model for beam correction at the WALS BITL. There are 30 quadrupole magnets that can be adjusted and limited locations to place beam profile monitoring systems for diagnostics along the BITL. It is expected that the neural network can tell K-values of quadrupoles to give the needed horizontal beam sizes (σ_x) and vertical beam sizes (σ_y) at the beam profile monitoring systems.

In the beam transfer line, it is known that the forward process from the magnet K-value to the beam size σ is accurately defined, but the inverse process from the beam size σ to the magnet K-value is vague, and there is even the possibility of a "many-to-one" solution. Therefore, an INN model has been designed to correct the beam at the WALS BITL. Through the forward learning of the network model, the K-value of

quadrupole magnets can predict the beam size, meanwhile, through the invertible mapping of the network model, the K-value of 30 quadrupole magnets corresponding to expected beam sizes can also be predicted. The network can not only realize the forward prediction from the magnet K-value to the beam size, but also realize the inverse prediction from the beam size to the magnet K-value, and the inverse prediction is based on the forward prediction. The forward learning process is in line with the physical nature of the beam dynamics along the WALS BITL, and the inverse prediction results are also highly accurate. So this method is efficient for the actual beam commissioning of the WALS BITL.

Beam size is considered as a learning feature for the following considerations: (1) It can be easily collected by beam profiles; (2) To ensure that the electrons are efficiently transported and not lost, beam size is the primary goal of beam commissioning; (3) Since the storage ring has strict requirements on beam dispersion when injecting the electron beam, the dispersion function is also an important target of correction. Beta function and other optical parameters should also be considered, since it can be seen from Equation 1 that the beam size is determined by the Beta function and the dispersion function. Considering the actual situation of the WALS BITL, in order to save beam diagnostic elements to the greatest extent, the beam size is selected, which can be expressed as

$$\sigma_i^2 = \beta_i \varepsilon_i + (\eta_i \sigma_e)^2 \tag{1}$$

where σ_i is the beam size, β_i is the Beta function, ϵ_i is the beam emittance, η_i is the dispersion function, σ_e is the energy spread (i refers to the horizontal or vertical). It can be seen from the equation that the beam size is changed along with the Beta function and dispersion function when the beam emittance and energy spread are constant.

The Adam optimization algorithm is introduced as an optimizer. The Adam optimization algorithm is different from the common stochastic gradient descent algorithm. It combines an adaptive learning rate and a momentum approach to efficiently and automatically adjust the learning rate and the speed of parameter updates during the training process. Back-propagation algorithm is chosen to compute the gradient function. Compared with forward propagation, which transmits the input data forward to the output layer, back-propagation is based on the chain rule, which finds the partial derivatives of all parameters and passes them backward, and constantly adjusts the weights and biases of the network, so that the neural network model can better fit the data and improve the generalization ability of the model [39].

Machine learning techniques are usually applied to accelerator physics using Artificial Neural Network (ANN). However, considering the unique characteristics of the WALS BITL, the INN model is chosen. Since the electron beam motion in the transfer line is unidirectional, there is a possibility that a variety of quadrupole magnet combinations correspond to the same beam size. Therefore, the main goal of this study is to quickly obtain a feasible combination of K-values of quadrupole magnets based on the desired target of the given beam size. The INN model is very suitable for this function, because its forward learning process can simulate the beam transport more accurately, and its inverse transmission process can quickly obtain a feasible K-values combination.

B. Beam Correction Process

The overall learning process of the INN model is shown in Fig. 7. There are mainly 5 steps lasting from Fig. 7(a) to (c). In Fig. 7(a) there are: Step 1, the AT toolbox of MATLAB is used to model the transfer line, where the injection parameter errors from the LINAC and magnets installation errors are randomly generated within the error ranges to make error seeds; Step 2, beam orbit is corrected with HVC magnets in simulation (in reality, orbit correction can be completed in the transfer line without machine learning); Step 3, multiple sets of quadrupole magnet K-value are randomly generated for each error seed, and the horizontal (σ_x) and vertical(σ_y) beam sizes simulated by AT (or measured during actual beam commissioning) at each profile are collected. K-values and beam sizes are treated as input x and output y, respectively, to form a dataset for learning (the ratio of training set, validation set and test set is 4:1:1.25). In Fig. 7(b) there is Step 4: with the error seed of No.1, the model is preliminarily trained, and the network structure and related hyperparameters are continuously adjusted to design the most reasonable model. At Step 5 as shown in Fig. 7(c), the model usability is verified: the dataset made by error seed is learned and predicted, and if the prediction result is reasonable, this error seed will be replaced by the next one. If it is unreasonable, the hyperparameters of the model are re-set until the 10 error seeds can be reasonably predicted. Then the INN model is considered to have reasonable structure and sufficient usability, and the beam transfer line can be corrected in simulation. The R^2 (coefficient of determination) is selected as the criterion for judging the rationality of the prediction results. When the average value of the forward prediction R^2 is greater than 0.90 and the average value of the inverse prediction R^2 is greater than 0.85, the prediction result is considered accurate enough.The R^2 is described in the sec. V C.

C. Optimization of beam profile monitoring system settings

There are about 10 locations where beam profile monitoring systems can be installed in the WALS BITL, defined as No.1 to No.10 from the beginning to the end of the beamline. The specific distribution of locations is indicated in Fig. 1 using arrows. To save space and cost, the number of beam profiles should be reduced as much as possible on the premise of ensuring the beam correction accuracy. An optimization has been performed using the ideal error-free WALS BITL, starting from Step 3 as shown in Fig. 7(a). Table 1 illustrates R^2 for different profile number. Begin with a total of 10 beam profile monitoring systems, the number is continuously reduced to make comparisons.

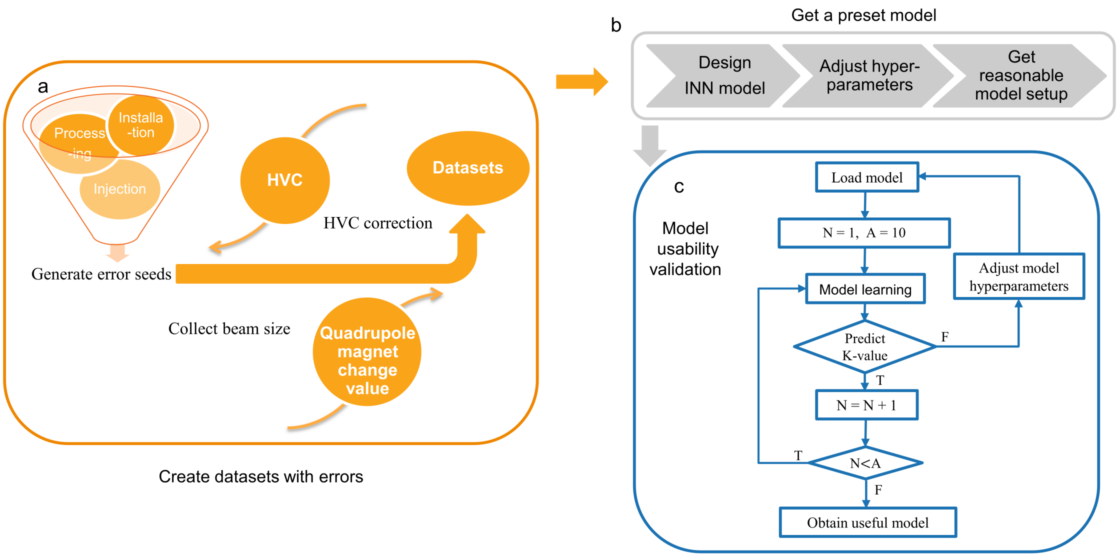

Fig. 7. Learning flowchart of the neural network system.

Table 1. Comparison of the R^2 with different number of beam profile monitoring systems

Profile number (position)	Forward prediction R^2	Inverse prediction R^2
10 (all)	0.9662	0.8442
8 (1-2-4-6-7-8-9-10)	0.9391	0.8296
7 (1-2-4-6-8-9-10)	0.9423	0.6797
6 (2-5-7-8-9-10)	0.9441	0.6933
5 (1-5-7-9-10)	0.9111	0.1817

Since the model uses the Adam optimizer, there are some fluctuations in R^2 value under this scheme. As can be seen from Table 1, when the number of profiles is reduced to 5, the inverse prediction R^2 value drops sharply. The fewer profiles are used, the fewer points can be observed, and less data can be learned by the model. Considering the practical requirements of the model and the cost of the devices, the number of profiles is finally determined to be 6. Considering that the application of the final model is to predict quadrupole magnet K-value according to wished beam size, a beam profile monitoring system must be placed in position No.10 behind the last quadrupole magnet. Because positions No.1, No.2, No.3, and No.4 are quite close to each other, and there are only a few quadrupole magnets nearby, one or two representatives should be enough for these four positions. On this basis, comparisons have been carried out between various combinations of 6 profile locations as listed in Table 2. Finally, positions No.1, No.4, No.5, No.6, No.8, and No.10 have been selected to make R^2 good enough.

D. Preparation of Datasets

The mainly considered errors of the WALS BITL include the injection errors at the start point of the BITL, for example, the Twiss parameter errors and position errors, the magnets installation errors, and magnetic field errors of dipoles and quadrupoles. Using the AT toolbox of MATLAB, the corresponding 10 error seeds are randomly generated. For each error seed, a dataset is produced for the neural network model to learn, where the input x are K-values of the quadrupole magnets and the output y are horizontal and vertical beam sizes at the 6 beam profile monitoring systems. Each dataset contains 10,000 groups of x and y. The ranges of the above errors are listed in Tables 3– 6. Specifically, Tables 3 and 4 show the positioning and Twiss parameter error ranges of the injected beam from the LINAC. Table 5 shows the considered installation error ranges of the diode and quadrupole magnets. Table 6 lists the magnetic field error ranges of dipoles and quadrupoles. The 10 random error seeds are generated within the error ranges listed in Tables 3– 6. For each error seed, the dataset containing K-values of the quadrupoles is produced for the neural network model based on the value listed in Table 6.

Ten random error seeds have been selected to verify whether the model structure and hyperparameter settings of the INN model are appropriate. If the model can successfully correct the beam under ten different error seeds, it also proves that the model has good versatility.

E. Design of the Network Structure

After comprehensive considerations, an INN model with 8 affine coupling modules has been designed, where the ReLU activation function is applied, and the Adam algorithm and

Table 2. Comparison between various combinations of 6 beam profile monitoring system positions

Profile position	Forward prediction R^2	Inverse prediction R^2
2-5-7-8-9-10	0.8328	0.7317
1-3-5-7-9-10	0.9146	0.5795
1-4-6-8-9-10	0.9395	0.6994
1-5-6-8-9-10	0.9394	0.8372
1-4-5-6-8-10	0.9290	0.9255

Table 3. Assumed positioning errors of the injected beam from the LINAC

Direction	Distance(mm)	Angle(mrad)
Horizontal	±0.5	±0.3
Vertical	±0.5	±0.3

Table 4. Assumed Twiss parameter errors of the injected beam from the LINAC

Direction	$\beta(\%)$	α	η(m)
Horizontal	±30	±0.3	±0.03
Vertical	±30	±0.3	±0.03

the Back-propagation algorithm are introduced. Fig. 8 shows the schematic diagram of the neural network structure.

F. Training Results

The prediction results of test set are visually analyzed, where the true value of beam size, the predicted values of both forward and inverse process are compared. The Box−plot [53] is applied for visual analysis. The Box−plot can clearly and straightforwardly display the quartile of the data, and hence reflect the distribution of data more realistically. As can be seen from Fig. 9, for the beam size, the median error is not more than 0.015 mm between the forward, inverse and true values, while 75% and 25% of the data, as well as the maximum and minimum values are almost symmetrically distributed on both sides of the median.

For the forward prediction, the result of σ_{3_y} is about 0.015 mm larger than the inverse and true values as a whole. However, in fact the model is used eventually with inverse prediction, so the difference between the inverse process and the true value is more concerned. As can be seen, the difference between the data distributions of the inverse predicted value and the true value is negligible at each beam profile monitoring system.

Fig. 10 is a comparison of the prediction and true values of the beam sizes at the first and the last beam profile monitoring locations. Each point in the figure corresponds to an individual in the test set. From Fig. 10, the minor deviations between the true values and the predicted values can be seen more transparently and informatively.

IV. VERIFICATION

Since the WALS BITL has not been built yet, MATLAB has been used to model it for virtual verification.

Fig. 11 shows a comparison of beam parameters before and after correction using the INN model with an error seed and $\pm1\%$ field error of quadrupoles. The continuous lines represent the resulted dispersion function and beam size under the above mentioned errors, while the dark blue dotted lines marked with circles show the corrected beam parameters using the INN model. As can be seen in Fig. 11, both the dispersion function and the beam size are well corrected. At the exit of the transfer line, the horizontal and vertical dispersion is 0.03 m, the horizontal beam size is 0.14 mm, and the vertical beam size is 0.12 mm.

Table 7 lists the comparison of beam sizes between the expected values and the corrected ones using INN. The input values refer to the beam sizes expected and imported to the INN model. According to the input values, the INN model predicts the K-values directly, and the corrected beam sizes are calculated by MATLAB using the WALS BITL with the predicted K-values of INN. The corrected beam sizes are very close to the expected values. Figure 11 and Table 7 further verify the accuracy of the INN model.

Fig. 12 shows beam dispersion function and beam size after correction using INN model for ten error seeds. The segmented blue curves represent theoretical or the ideal beam parameters along the transfer line without error. The continuous curves in color show the corrected results using the INN model under the ten error seeds. As can be seen from Fig. 12, the corrected dispersion function and beam size are close to the ideal condition. The dispersion function at the exit of the transfer line is within 0.15 m, and the beam size can be corrected to be within 0.3 mm.

By comparing Fig. 12 and Fig. 6, it is observed that: in the x-direction,the global correction method corrects the dispersion function at the endpoint within 0.01 m, while the INN model corrects it to within 0.1 m. In the y-direction, the global correction method corrects the dispersion function at the endpoint close to 0 m, while the INN model corrects it to within 0.15 m. Both of the two methods meet the correction requirement of 0.2 m. Although the global correction method can achieve more precise correction effects in simulation environments, this method is limited to simulations because it requires more beam information than what can be provided by actual beam diagnostic systems. In contrast, the INN model is specifically designed for practical beam correction applications and can effectively utilize limited beam diagnostic information for correction. This capability for practical application makes the INN model more advantageous in

Table 5. Assumed installation errors of dipoles and quadrupoles in the WALS BITL

Magnet type	Horizontal installation(mm)	Vertical installation(mm)	Longitudinal installation/(mm)	Rotation in the x-direction(mrad)	Rotation in the y-direction(mrad)	Rotation in the z-direction(mrad)
Dipole	± 0.5	± 0.2	± 0.5	± 0.5	± 0.5	± 0.2
Quadrupole	± 0.2	± 0.2	± 1.0	± 0.5	± 0.5	± 0.5

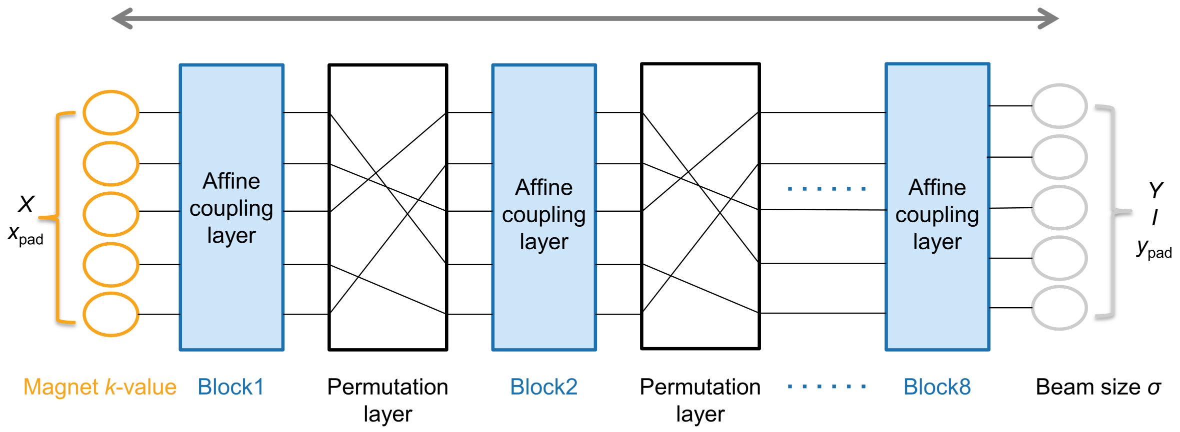

Fig. 8. Diagram of the neural network structure.

Table 6. Assumed Magnetic field errors of dipoles and quadrupoles in the WALS BITL

Magnet type	Magnetic field error(%)
Dipole	± 0.1
Quadrupole	± 0.2

actual operations, especially when beam information is limited. Therefore, despite the global correction method's excellent performance in simulations, the feasibility and flexibility of the INN model in practical applications make it a more practical choice.

V. METHOD ANALYSIS

The code programming of the INN model designed in this paper is based on previous work [54]. The following is an analysis of the method applied in the WALS BITL. Sec. V A introduces the dynamic relationships in the WALS BITL, and analyzes the mathematical relationships of the INN model applied to the WALS BITL. Sec. V B provides a detailed description of the considerations for selecting the loss function in neural networks, with Table 8 summarizing the hyperparameters used in the final model. Sec. V C introduces the R^2 and steps of evaluating the model.

A. Dynamic Relationships

The dynamic equations for the particle beam and the quadrupole magnet K-values at the WALS injection transfer line is

$$\hat{f} : D^{\vec{K}} \times D \to D^{\vec{\sigma}} \tag{2}$$

$$\hat{f}(\vec{k}, d) = \hat{\sigma}(d) \tag{3}$$

where K represents the value of the quadrupole magnet, $d \in D$ represents the location in the beamline, function $\hat{f}$ represents the transfer line model, $\hat{\sigma}$ represents the electron beam size at the location d.

INN model generally requires that the input and output data dimensions are the same. However, for the problem discussed in this paper, the input data dimension is 30 while the output data dimension is 12, which are unequal, so it is necessary to compensate the data dimensions. Here, we define the total data dimension as A. Since the solution of the inverse problem is not unique, and there is a possibility of many-to-one solutions, when solving, it is not only mapped to the pre-designed values, but also mapped to a prospective spatial distribution (I distribution) that has been learned. Via randomly sampling in I, the model constantly tries to find the most suitable distribution value to complete the optimal solution of the inverse problem [54]. The total dimension A can be described as

$$A = dim\,(K) + 1 + dim\,(x_{pad}) = dim\,(\sigma) + dim\,(y_{pad}) + I \tag{4}$$

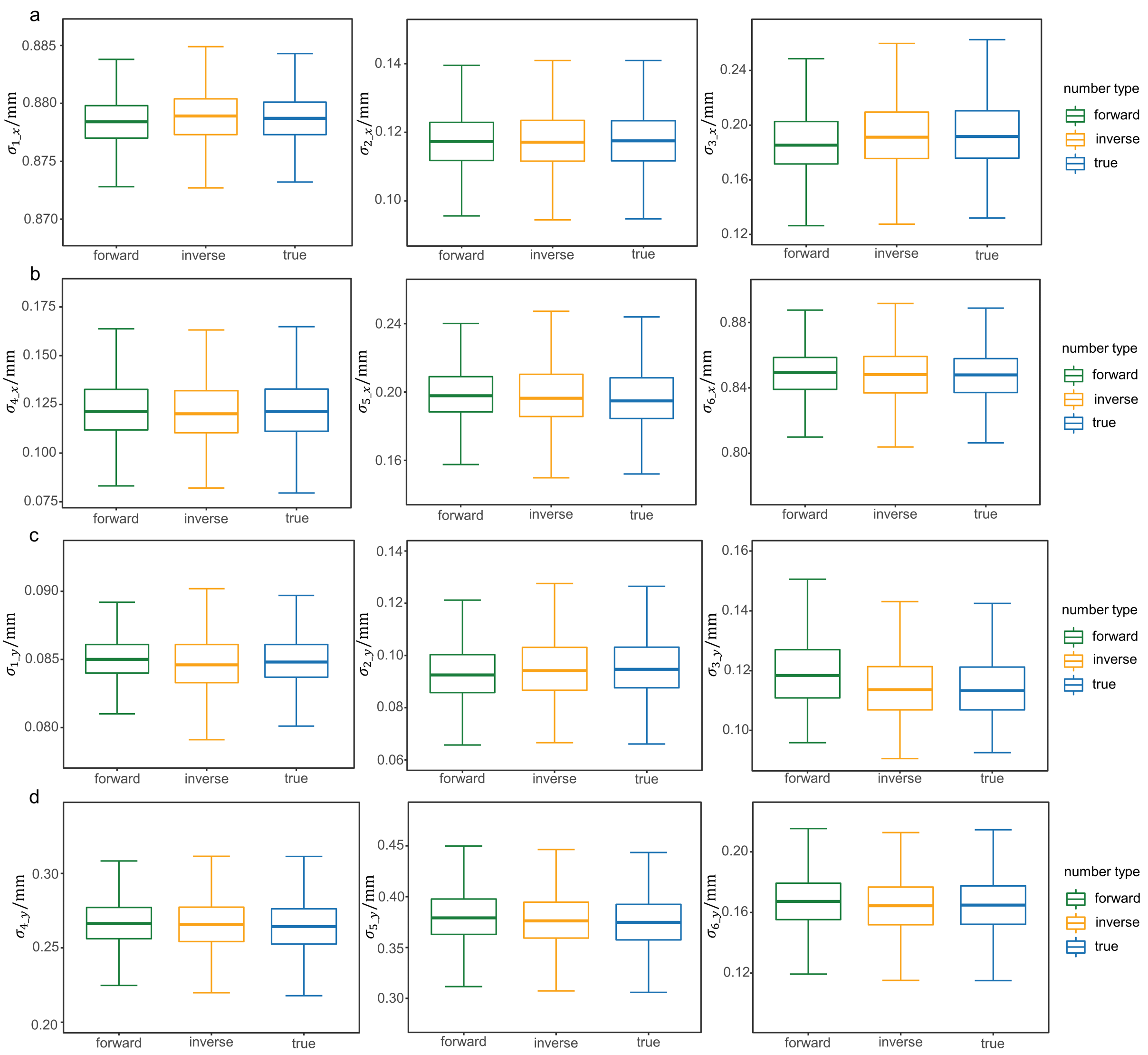

Fig. 9. Comparisons of beam sizes between true value and predicted values at the 6 beam profile monitoring systems.

Table 7. Comparison of beam sizes between the expected values and the corrected ones

Value type	Direction	σ_1(mm)	σ_2(mm)	σ_3(mm)	σ_4(mm)	σ_5(mm))	σ_6(mm)
Input	x	0.7546	0.1630	0.0667	0.1406	0.2107	0.9885
	y	0.1145	0.1359	0.9122	0.0928	0.1785	0.1049
Corrected	x	0.7528	0.1623	0.0729	0.1500	0.2127	0.9956
	y	0.1153	0.1364	0.9108	0.0932	0.1812	0.1040

where x_{pad} is the complementary dimension of the input data and y_{pad} is the complementary dimension of the output data. I is the potential spatial distribution dimension. For this paper, only the dimensionality of the output data is supplemented, so the mathematical expression of the forward prediction of the physical model for the transfer line is

$$\hat{f} : D^{\vec{K}} \times D \to D^{\vec{\sigma}} \times D^{\dim(y_{pad})} \times D^{I} \tag{5}$$

$$\hat{f}(\vec{k}, d) = (\hat{\sigma}(d), \dim(y_{pad}), I) \tag{6}$$

The mathematical expression for the inverse prediction of the transfer line is

$$\hat{f}^{-1} : D^{\vec{\sigma}} \times D^{\dim\,(y_{pad})} \times D^{I} \to D^{\vec{K}} \times D \tag{7}$$

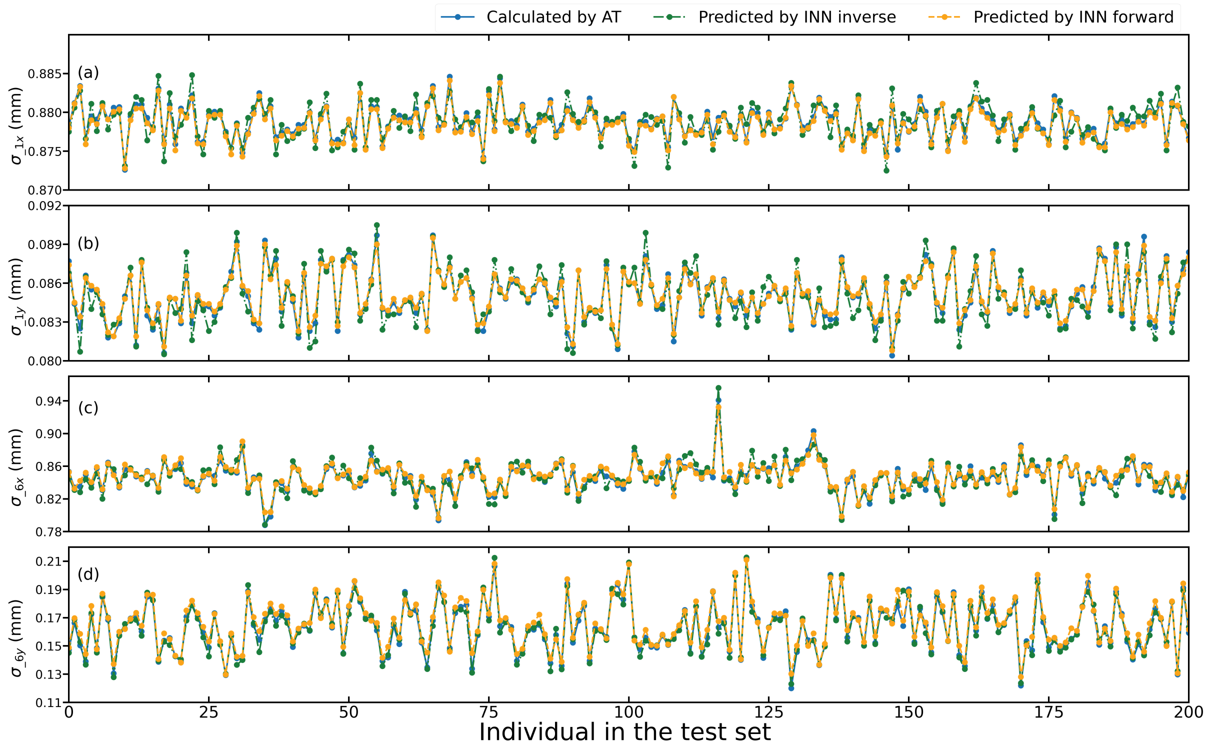

Fig. 10. Comparison chart of predicted and true beam sizes at the first and the last beam profile monitoring systems. "Calculated by AT" represents the true value, "Predicted by INN forward" represents the predicted value (forward), and " Predicted by INN inverse" represents the predicted value (inverse).

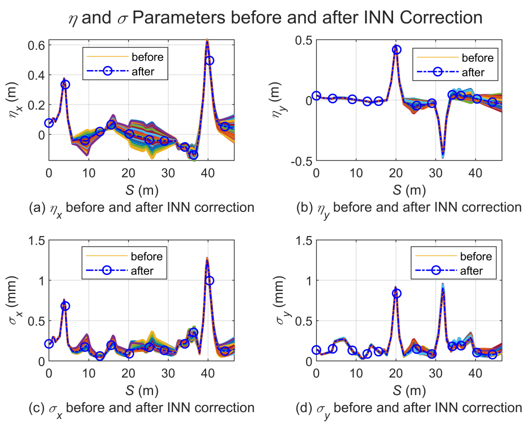

Fig. 11. Beam dispersion function and beam size before and after correction using INN model under errors. The solid colorful lines represent results before correction, while the dash-dotted lines are results after correction.

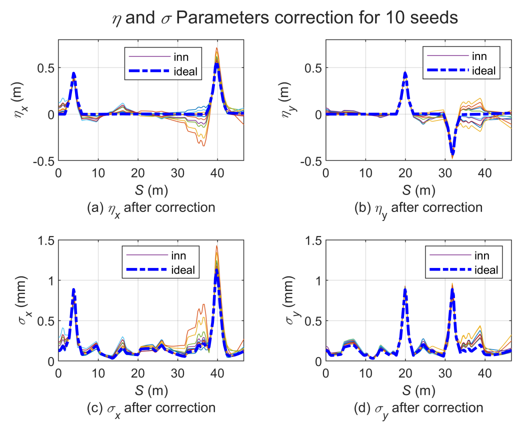

Fig. 12. Beam dispersion function and beam size after correction using INN model for ten error seeds.The solid colorful lines represent results after the INN correction, while the dash-dotted lines plot ideal values needed.

$$\hat{f}^{-1}(\hat{\sigma}(d), \dim(y_{pad}), I) = (\vec{k}, d) \tag{8}$$

B. Loss Function

The definition of the loss function during training consists of five components: the mean square error L_{MSE} between the predicted output and the true value of the model, the mean square error L of the complementary dimensions of the out-

put data, the reconstruction error L_r in order to reduce the influence of small perturbations (δ) on it in the reverse prediction, L_k which is used to ensure that the sampled magnet K-values follow the same distribution as the data set, and L_I which is used to ensure that the potential spatial distribution D^I follows the desired one. Expression for the loss function is

$$L_{all} = \omega_{MSE} L_{MSE} + \omega_r L_r + \omega_\alpha L_\alpha + \omega_k L_k + \omega_I L_I \tag{9}$$

where ω_{MSE}, ω_r, ω_α, ω_k, and ω_I are the percentage weights of the corresponding errors.

The mean square error MSE equation and the reconstruction error equation are as

$$MSE = \frac{1}{n} \sum_{i=1}^{n} (y_i - \hat{y}_i)^2 \tag{10}$$

$$L_r = \sum_{i=1}^{n} \left(\hat{f}^{-1} \left(\hat{f}(k_i, d_i) + \delta \right) - k_i \right)^2 \tag{11}$$

In the above equations, n is the total value of quadrupole magnets in each sample, i.e., 30. Table 8 shows the other detailed data configurations corresponding to the INN model.

Table 8. Configurable parameters related to the INN model

INN model parameter configuration of the WALS BITL	
Data preprocessing	$x \in$[0,1] $y \in$[0,1]
Potential spatial distribution dimensions	I = 1
Loss function weights	ω_{MSE}=50 ω_r=10 ω_α=1 ω_k=50 ω_I=50
Optimization algorithm	Adam
Activation function	ReLU function
Number of trainable elements	137792
Number of blocks of affine coupling layers	8
Learning rate	0.002
Sample batch Size	32
Epochs	50

C. Evaluation Indicators

At the end of the transfer line, beam size is determined by all the quadrupole magnets in the entire beamline (there are also the influences of dipoles, which are ignored here), so in the inverse prediction, simply comparing the predicted value with the real value cannot truly reflect the accuracy of the model. Therefore, the R^2 has been determined as the evaluation index. The value range of R^2 is between 0$\sim$1, and the closer it is to 1, the higher the prediction accuracy of the model is. R^2 is expressed as

$$R^2 = 1 - \frac{\sum_i (\hat{y}_i - y_i)^2}{\sum_i (\bar{y}_i - y_i)^2} \tag{12}$$

where y_i is the true value, $\bar{y}_i$ is the average of the true value, $\hat{y}_i$ is the predicted value.

The steps to evaluate the model are as follows: (1) The model makes a forward prediction of the validation set and obtains the forward prediction σ value corresponding to the K-value of the quadrupole magnets (true K-value); (2) The true σ value and the forward prediction of σ value are used to calculate the R^2 of the forward prediction; (3) The model makes an inverse prediction of validation set and obtains the K-value of the quadrupole magnets predicted corresponding to the true σ ; (4) The model makes a forward prediction of the K-value of the quadrupole magnets that has been predicted, and obtains the σ value of the inverse prediction; (5) The true σ value and the σ value of the inverse prediction are used to calculate R^2 of the inverse prediction. Fig. 13 shows the specific steps. Among them, the Inverse prediction-σ obtained by the Pending K-value after the forward prediction represents the predicted σ value of the whole inverse prediction process.

After adequate tests, the value of R^2 can reach a maximum of about 0.96 for forward prediction and about 0.93 for inverse prediction. From either the corrected Twiss parameters and beam sizes, or the R^2 value, the feasibility of this INN model for the beam correction study of the WALS BITL can be confirmed. Table 9 lists the R^2 data for an error seed. As can be seen from the table, the average forward prediction $\bar{R}^2$ reaches 0.9483, and for the inverse prediction, $\bar{R}^2$ reaches 0.9342.

VI. CONCLUSIONS

An INN model has been designed by using machine learning neural network algorithm to carry out the optimization study of beam correction for the WALS BITL. The method has been proved to be feasible and the beam correction effect is remarkable in simulations. In view of the unique "three-stage" design of the WALS BITL, the neural network algorithm can not only solve the problem of simultaneous beam correction horizontally and vertically, but also solve the beam correction difficulty caused by the lack of beam information under limited measurement points. The final design of the INN model not only realizes the forward prediction from the

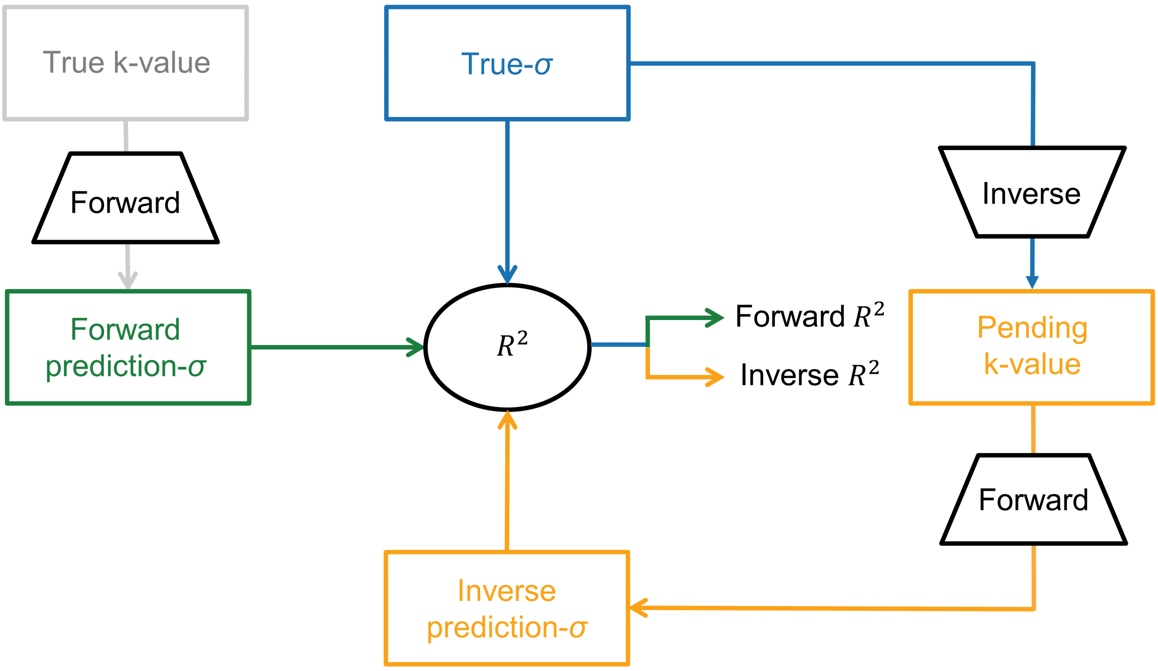

Fig. 13. Flow chart to evaluate the INN model of the WALS BITL.

Table 9. R^2 enumeration table

	Direction	σ_1	σ_2	σ_3	σ_4	σ_5	σ_6	Average value
Forward	x	0.9637	0.9600	0.9006	0.9178	0.9613	0.9381	0.9403
	y	0.9761	0.9768	0.9099	0.9578	0.9581	0.9584	0.9562
Inverse	x	0.8618	0.9558	0.9730	0.9570	0.9594	0.8488	0.9260
	y	0.8803	0.9224	0.9584	0.9506	0.9631	0.9787	0.9423

magnet K-value to the beam size σ, but also realizes the inverse prediction from the beam size σ to the K-value of the quadrupole magnet. The AT toolbox of MATLAB has been used to model the transfer line, collect the beam related data, verify the inverse prediction results of the INN model, and finally successfully realize the commissioning optimization of the WALS BITL in simulation. This method can provide visual guidance for the actual beam correction process. In the future, we will further explore the possibility of designing a proper INN model with reduced number of beam profile monitoring systems in the beamline to save construction cost. During the construction and commissioning of the WALS BITL, the method will be applied in practice. In this paper, machine learning algorithm is studied for the beam correction of the WALS BITL, the strategy may be applied to similar accelerator physics problems in other facilities.

Acknowledgments: This work was supported by the Major Science and Technology Project of Hubei Province (2021AFB001).

Author Contributions: All authors contributed to the study conception and design. Material preparation, data collection and analysis were performed by Hui Wang, Hao-Hu Li, Jiao-Bao Guan and Yuan-Cun Nie.The first draft of the manuscript was written by Hui Wang, Hao-Hu Li and Yuan-Cun Nie reviewed and edited the manuscript. All authors commented on previous versions of the manuscript. All authors read and approved the final manuscript.

Data availability: The data that support the findings of this study are available from the corresponding author upon reasonable request.

DECLARATIONS

Conflict of Interest: The authors declare that they have no conflict of interest.

REFERENCES

[1] H.N. Chapman, Fourth-generation light sources. IUCrJ **10**, 246 (2003). doi: 10.1107/S2052252523003585

[2] P.F. Tavares, E. Al-Dmour, A. Andersson, et al., Commission-

ing and first-year operational results of the MAX IV 3 GeV ring. J. Synchrotron Rad. **25**, 1291 (2018). doi: 10. 1107/ S1600577518008111
[3] Y. Jiao, Z.H. Bai, X. Li, Accelerator physics and technology of the fourthgeneration synchrotron radiation light source. PHYSICS **53**, 71 (2024). doi:10.7693/wl20240201(in Chinese)
[4] L. Valle, T. Brochard, N. Carmignani, et al., Off-energy operation for the Extremely Brilliant Source at the European Synchrotron Radiation Facility. Phys. Rev. Accel. Beams **27**, 051601 (2024). doi:10.1103/PhysRevAccelBeams.27.051601
[5] J. Yi, X. Gang, X.H. Cui, et al., The HEPS project. J. Synchrotron Rad. **25**, 1611 (2018). doi10.1107/S1600577518012110
[6] Z.H. Bai, G.W. Liu, T.L. He, et al., A Modified Hybrid 6BA Lattice for the HALF Storage Ring. Paper Presented at the IPAC 2021, Campinas, SP, Brazil, August 2021, pp. 407-409. doi:10.18429/JACOW-IPAC2021-MOPAB112
[7] F.C. Li, R.Z. Liu, W.J. Li, et al., Synchrotron radiation: A key tool for drug discovery. Bioorg. Med. Chem. Lett. **144**, 129990 (2024). doi: 10.1016/j.bmcl.2024.129990
[8] Z.Y. Dai, Y.C. Nie, Z. Hui, et al., Design of S-band photoinjector with high bunch charge and low emittance based on multi-objective genetic algorithm. Nucl. Sci. Tech. **34**, 41 (2023). doi:10.1007/s41365-023-01183-6
[9] H.H. Li, J. Wang, L. Tang, et al., Project of Wuhan photon source. Paper Presented at the IPAC 2021, Campinas, SP, Brazil, August 2021, pp. 346-349.doi:10.18429/JACOW-IPAC2021-MOPAB092
[10] Y. Zou, H.H. Li, Y. Chen, et al., Studies on beam injection system for Wuhan advanced light source storage ring. Paper Presented at the IPAC 2023, Venice, Italy, September 2023, pp. 1176-1179. doi:10.18429/JACoW-IPAC2023-MOPM086
[11] Z.Y. Dai, Y.C. Nie, J.H. Zhong, et al., Beam dynamics study of the photoinjector at Wuhan advanced light source. Radiation Detection Technology and Methods **8**, 1319 (2024). doi:10.1007/s41605-024-00455-y
[12] H.H. Li, J. Li, G. Wei, et al., Beam transfer line of Wuhan advanced light source. Paper Presented at the IPAC 2023, Venice, Italy, May 2023, pp. 1082-1084. doi:10.18429/JACoW-IPAC2023-MOPM040
[13] A.G. Akritas, G.I. Malaschonok, Applications of singular-value decomposition (SVD). Math. Comput. Simulat. **67**, 15 (2004). doi:10.1016/j.matcom.2004.05.005
[14] S.H. Mirza, R. Singh, P. Forck, et al., Closed orbit correction at synchrotrons for symmetric and near-symmetric lattices. Phys. Rev. Accel. Beams **22**, 072804 (2019). doi:10.1103/PhysRevAccelBeams.22.072804
[15] A.M. Coxe, J.F. Benesch, R.M. Bodenstein, et al., Beam correction for multi-pass arcs in FFA @ CEBAF: status update. Paper Presented at the IPAC 2024, Nashville, TN, July 2024, pp.1054-1056. doi:10.18429/JACoW-IPAC2024-TUPC23
[16] H. Jin, D.O. Jeon, J.H. Jang, Results of on-line orbit correction at the medium energy beam transport section of the RAON accelerator. J. Korean. Phys. Soc. **83**, 854 (2023). doi:10.1007/s40042-023-00919-2
[17] J. Arthur, G. Materlik, R. Tatchyn, et al., The LCLS: A fourth generation light source using the SLAC linac. Rev. Sci. Instrum. **66**, 1987 (1995). doi:10.1063/1.1145778
[18] J.N. Galayda,The LCLS-II: A high power upgrade to the LCLS. Paper Presented at the IPAC 2018, Vancouver, BC, Canada, June 2018, pp. 18-23. doi:10.18429/JACoW-IPAC2018-MOYGB2
[19] C. Emma, A. Edelen, M.J. Hogan, et al., Machine learning-based longitudinal phase space prediction of particle accelerators. Phys. Rev. ST Accel. Beams. **22**, 112802 (2018). doi:10.1103/PhysRevAccelBeams.21.112802
[20] H.J. Xu, Z.T. Zhao, Current status and progresses of SSRF project. Nucl. Sci. Tech. **19**, 1 (2018). doi:10.1016/S1001-8042(08)60013-5
[21] T.Y. Yang, W. Wen, G.Z. Yin, et al., Introduction of the X-ray diffraction beamline of SSRF. Nucl. Sci. Tech. **26**, 020101 (2015). 10.13538/j.1001-8042/nst.26.020101
[22] Z.L. Li, Y.C. Fan, L. Xue, et al., The design of the test beamline at SSRF. AIP Conf. Proc. **2054**, 060040 (2019). doi:10.1063/1.5084671
[23] J.H, He, X.Y. Gao, Status of the crystallography beamlines at SSRF. Eur. Phys. J. Plus. **130**, 1 (2015). doi:10.1140/epjp/i2015-15032-6
[24] R.C. Li, Q.L. Zhang, Q.R. Mi, et al., Application of machine learning in orbital correction of storage ring. High Power Laser and Particle Beams **33**, 034007 (2021). doi:10.11884/HPLPB202133.200318(in Chinese)
[25] T. J. Kattenborn, J. Leitloff, F. Schiefer, et al., Review on Convolutional Neural Networks (CNN) in vegetation remote sensing. ISPRS. J. Photogramm. **173**, 24 (2021). doi:10.1016/j.isprsjprs.2020.12.010
[26] L. Alzubaid, J.L. Zhang, A.J. Humaidi, et al., Review of deep learning: concepts, CNN architectures, challenges, applications, future directions. J. Big Data. **8**, 1 (2021). doi:10.1186/s40537-021-00444-8
[27] W.C. Zhu, Z.Y. Wei, C.J. Xie, et al., Development of the NFTHz accelerator beam profile measurement system. High Power Laser and Particle Beams. **36**, 034004 (2024). doi:10.11884/HPLPB202436.230361(in Chinese)
[28] H. Zou, The adaptive lasso and its oracle properties. J. Am. Stat. Assoc. **101**:1418 (2006). 10.1198/016214506000000735
[29] J. Ranstam, J.A. Cook, LASSO regression. Brit. J. Surg. **105**, 1348 (2018). doi:10.1002/bjs.10895
[30] Y.B. Yu, W.B. Ni, G.F. Liu, et al., Initial Application of Machine Learning for Beam Parameter Optimization at the Hefei Light Source II. J. Phys. Conf. Ser. **2687**, 072002 (2024). doi:10.1088/1742-6596/2687/7/072002
[31] Z.M. Chu, D.J. Xiao, Y.S. Qiao, et al., Machine Learning Applications for Particle Accelerators. Front. Data. Comput. **1**, 110 (2019). doi:10.11871/jfdc.issn.2096-742X.2019.02.010
[32] Y.B. Yu, G.F. Liu, W. Xu, et al., Research on tune feedback of the Hefei Light Source II based on machine learning. Nucl. Sci. Tech. **33**, 28 (2022). doi:10.1007/s41365-022-01018-w
[33] L. Ardizzone, J. Kruse, S.J. Wirkert, et al., Analyzing inverse problems with invertible neural networks. Paper Presented at the ICLR 2019, Ernest N. Morial Convention Center. February. 2019. 10.48550/arXiv.1808.04730
[34] O. Moran, P. Caramazza, D. Faccio, et al., Deep, complex, invertible networks for inversion of transmission effects in multimode optical fibres. Paper Presented at Neur. IPS 2018, Montreal, Canada, December, 2018. doi:10.5555/3327144.3327248
[35] D.P. Kingma, P. Dhariwal, Glow: Generative flow with invertible 1x1 convolutions. Paper Presented at Neur. IPS 2018. Montreal, Canada, December, 2018. pp. 10236-10245. doi:10.5555/3327546.3327685
[36] D. Yarotsky, Error bounds for approximations with deep ReLU networks. Neural networks. **94**, 103 (2017). doi:10.1016/j.neunet.2017.07.002
[37] J.C. He, L. Lin, J.C. Xu, et al., ReLU deep neural networks and linear finite elements. J. Comput. Math. **38**, 502 (2020). 10.4208/jcm.1901-m2018-0160

[38] D.P. Kingma, J. Ba, Adam: A method for stochastic optimization. Paper Presented at ICLR 2015, San Diego. May 2015. doi:10.48550/arXiv.1412.6980

[39] D.E. Rumelhart, G.E. Hinton, R.J. Williams, Learning representations by back-propagating errors. Nature. **323**, 533 (1986). doi:10.1038/323533a0

[40] J. Li, J.H. Cheng, J.Y. Shi, et al., Brief introduction of back propagation (BP) neural network algorithm and its improvement. Advances in Computer Science and Information Engineering: Volume 2. (Springer, Berlin Heidelberg, 2012), pp. 553-558.

[41] S. Walston, S. Boogert, C. Chung, et al., Performance of a high resolution cavity beam position monitor system. Nucl. Instrum. Meth. A. **578**, 1 (2007). doi:10.1016/j.nima.2007.04.162

[42] Y.C. Wu, J.W. Feng, Development and application of artificial neural network. Wirel. Pers. Commun. **102**, 1645 (2018). doi:10.1007/s11277-017-5224-x

[43] B.C. Wang, C.X. Tang, M.T. Qiu, et al., A machine learning approach to TCAD model calibration for MOSFET. Nucl. Sci. Tech. **34**, 192 (2023). doi:10.1007/s41365-023-01340-x

[44] Y.J. Ma, Y. Ren, P. Feng, et al., Sinogram denoising via attention residual dense convolutional neural network for low-dose computed tomography. Nucl. Sci. Tech. **32**, 41 (2021). doi:10.1007/s41365-021-00874-2

[45] X.D. Guo, P. He, X.J. Lv, et al., Material decomposition of spectral CT images via attention-based global convolutional generative adversarial network. Nucl. Sci. Tech. **34**, 45 (2023). doi:10.1007/s41365-023-01184-5

[46] G.X. Wei, S.X. Zhang, Z. Li, et al., Multi-modality measurement and comprehensive analysis of hepatocellular carcinoma using synchrotron-based microscopy and spectroscopy. Nucl. Sci. Tech. **32**, 102 (2021). doi:10.1007/s41365-021-00927-6

[47] H.Y. Yang, D. Wang, D.D. Wang, An overview of the application of neural network algorithm in the nuclear field of China. Nucl. Sci. Tech. **8**, 19 (2020). doi:10.12677/NST.2020.81003(in Chinese).

[48] W.B. He, Y.G. Ma, L.G. Pang, et al., High-energy nuclear physics meets machine learning. Nucl. Sci. Tech. **34**, 88 (2023). doi:10.1007/s41365-023-01233-z

[49] Z.P. Gao, Y.J. Wang, H.L. Lü, et al., Machine learning the nuclear mass. Nucl. Sci. Tech. **32**, 109 (2021). doi:10.1007/s41365-021-00956-1

[50] Y. Zou, Q.Z. Xing, B.C. Wang, et al., Application of the asynchronous advantage actorcritic machine learning algorithm to real-time accelerator tuning. Nucl. Sci. Tech. **30**, 158 (2019). doi:10.1007/s41365-019-0668-1

[51] K. Deb, A. Pratap, S. Agarwal, et al., A fast and elitist multiobjective genetic algorithm: NSGA-II. IEEE Trans. Evol. Comput. **6**, 182 (2002). doi:10.1109/4235.996017

[52] H.X. Yin, J.B. Guan, S.Q. Tian, et al., Design and optimization of diffraction-limited storage ring lattices based on many-objective evolutionary algorithms. Nucl. Sci. Tech. **34**, 147 (2023). 10.1007/s41365-023-01284-2

[53] R. Mcgill, J.W. Tukey, W.A. Larsen. Variations of box plots. Am. Stat. **32**, 12 (1978). doi:10.1080/00031305.1978.10479236

[54] R. Bellotti, R. Boiger, A. Adelmann, Fast, efficient and flexible particle accelerator optimisation using densely connected and invertible neural networks. Information **12**, 351 (2021). doi:10.3390/info12090351